Diagnostics and experimental analysis of 3D printed concrete structural elements

Matěj Velát, Pavel Schmid, Petr Daněk, Richard Dvořák, Kristýna Hrabová
Brno University of Technology, Czechia
Matej.velat@vut.cz, https://orcid.org/0009-0006-8252-8002
Pavel.schmidt@vut.cz, http://orcid.org/0000-0001-8489-9452
Petr.danek@vut.cz, http://orcid.org/0000-0001-8489-9452
Richard.dvorak@vut.cz, https://orcid.org/0000-0003-0024-2344
Kristyna.hrabova@vut.cz, http://orcid.org/0000-0003-2078-1898

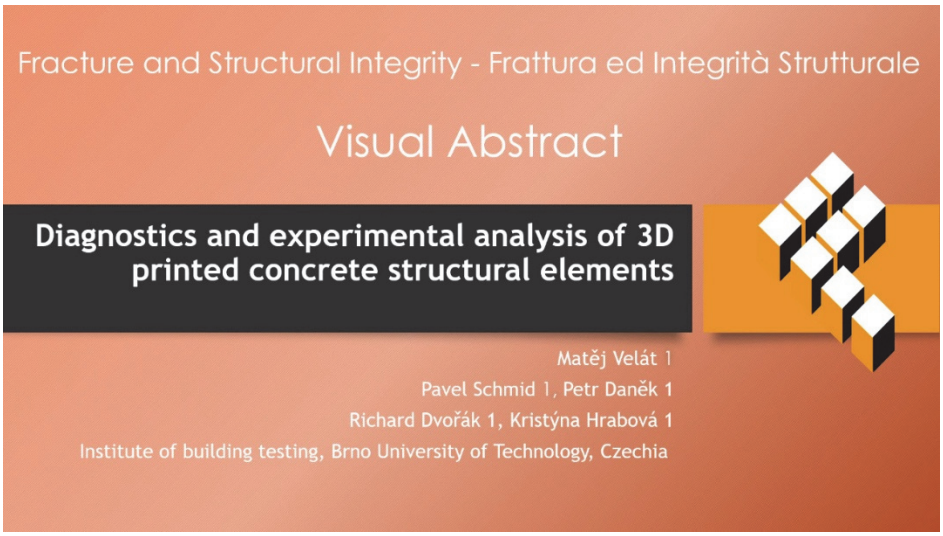

Citation: Velát, M., Schmid, P., Daněk, P., Dvořák, R., Hrabová, K., Diagnostics and experimental analysis of 3D printed concrete structural elementse, Fracture and Structural Integrity, 75 (2026) 339-350.

Received: 03.09.2025
Accepted: 17.10.2025
Published: 14.11.2025
Issue: 01.2026

KEYWORDS. 3D concrete printing (3DCP), Non-destructive testing (NDT), Mechanical properties, Anisotropy.

INTRODUCTION

Concrete is the most widely used construction material worldwide, second only to water in overall consumption [6]. Its popularity results from a combination of high compressive strength, durability, and versatility, which make it fundamental to infrastructure development. Traditionally, structural concrete is produced either cast in place or precast. Precasting enables better quality control and material properties due to optimized curing and compaction, while cast-in-place techniques provide flexibility for large monolithic structures. When executed properly, both conventional methods yield relatively homogeneous material, supported by well-established design codes and standardised testing procedures (e.g., compressive strength tests of cylinders or cubes, modulus of rupture tests)[4].
Over the past decade, 3D concrete printing (3DCP) has emerged as an innovative construction method that fabricates structures digitally by extruding cementitious mortar or concrete layer by layer, eliminating the need for formwork. This

additive approach offers reduced labour and formwork costs, faster construction, and the possibility of producing complex geometries. Reported applications range from architectural facades to structural components such as load-bearing walls, and research in this field is expanding rapidly [2]. However, 3DCP differs fundamentally from conventional casting in both the deposition process and the resulting internal structure. In contrast to cast or precast concrete, which is placed as a continuous mass, 3D-printed concrete is built up from discrete layers deposited sequentially. Each layer partially hardens before the next is applied, creating interfaces that frequently act as planes of weakness. These interfaces cause mechanical anisotropy, meaning that strength and stiffness depend on the loading direction relative to the print layers [5,7]. Moreover, the surface quality and geometric accuracy of 3DCP are determined by the extrusion process itself, often leading to ribbed surfaces and imperfections that would normally be avoided with conventional formwork. These characteristics complicate the application of conventional concrete testing methods. Standardised procedures for evaluating compressive strength, flexural behaviour, or ultrasonic properties are based on the assumption of isotropy and uniform material properties—assumptions that do not necessarily apply to 3DCP. The orientation of a specimen relative to the print layers can significantly influence the measured values: drilled cores or cut beams tested perpendicular to the layers often show lower strength than those tested parallel to the print direction [7,9]. Furthermore, non-destructive techniques such as ultrasonic pulse velocity (UPV) may not reliably detect weak interfaces unless carefully calibrated.

Another challenge is the absence of dedicated testing standards and building codes for 3D-printed concrete. Existing regulations, such as EN 12390 or ASTM C39, do not provide procedures for testing printed specimens or for interpreting anisotropic behaviour. Consequently, engineers often rely on case-specific adaptations and extensive experimental validation. This lack of normative guidance limits the broader adoption of 3DCP and hampers the development of systematic quality control and diagnostic procedures [2]. To address these issues, recent studies have explored both destructive and non-destructive evaluation methods for 3D-printed components, with particular attention to how anisotropy and print-related defects influence structural performance. Experimental research has confirmed that interlayer bonding is a decisive factor in both tensile and flexural strength and that diagnostic approaches must consider orientation-dependent behaviour. These findings underline the need for adapted testing protocols and assessment methods tailored to additive manufacturing. Motivated by these challenges, this paper presents an experimental study of full-scale 3D-printed concrete columns produced from a cement-based mortar using extrusion-based technology. The elements were tested in bending until failure, after which fragments were extracted for laboratory evaluation. Mechanical and physical properties, including compressive strength, flexural tensile strength in two orientations, ultrasonic pulse velocity, water absorption, and bulk density—were measured and analysed with respect to print orientation.

MATERIALS AND METHODS

Six structural columns were used for the experiment. All were printed using extrusion-based 3D printing with a cement-based mortar mixture. The exact material composition was unknown due to the time gap since printing, but the mix was designed for good printability and workability. Age of columns in time of testing was approximately 2 years from the printing. The total extruded filament length was 132 929.2 mm. The printing duration per specimen was 47.6 min, with an additional 5 min of preparation, resulting in a total processing time of 52.6 min per specimen. The cumulative printing time required for all specimens was 390.6 min (≈ 6.5 h). The columns were printed in a vertical orientation with visible print layers and surface imperfections. The illustration of specimen is shown in Fig. 1 (a). Each specimen was measured after printing in set dimensions shown in Fig. 1 (b).

Each column had approximate dimensions of 1000 mm in height, 800 mm in length, and 400 mm in width. The wall thickness was around 65 mm, corresponding to one printed path including surface ridges. The elements were printed with various intentional imperfections, such as uneven layer bonding and inconsistent printing speed. The list of all printed specimens is shown in Tab. 1. In addition to geometrical variations, several specimens were intentionally printed with different levels of imperfections to investigate their influence on structural behaviour. Specimens CP18-01, CP18-02, and CP18-03 were printed without visible defects and served as reference elements. Specimen CP18-04 contained a locally narrower filament along approximately one-third of the span through the entire wall thickness, most likely caused by a brief interruption of printing; the exact duration of this idle period was not recorded. Specimen CP18-05 exhibited a similar, locally reduced filament width on one of the longer sides over about one-third of the span, which was positioned on the upper surface during loading. Specimen CP18-06 was printed without any apparent defects. These intentional irregularities allowed the assessment of how printing discontinuities and reduced layer width affect stiffness, failure mode, and interlayer bonding quality.

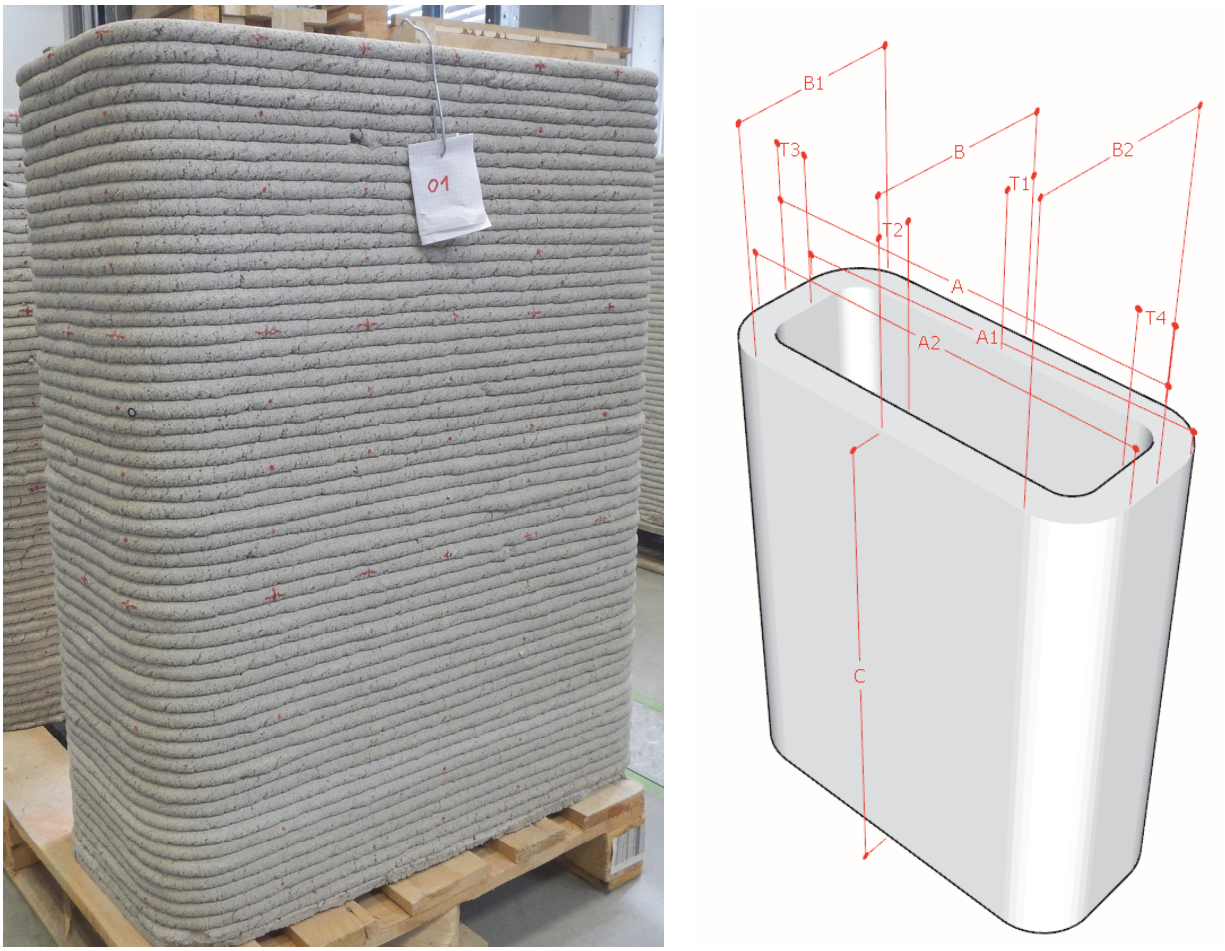

(a) (b)

Figure 1: Illustration of tested specimens (a) and the main measured dimensions (b)

Dimension (mm)	Specimens				
	CP18-01	CP18-02	CP18-03	CP18-04	CP18-05
A	820	818	820	815	810
A1	818	815	810	815	812
A2	815	820	820	810	810
B	365	365	370	365	365
B1	370	370	365	363	363
B2	363	365	370	368	363
C	1000	1000	980	985	1010
T1	70	70	70	65	68
T2	71	71	71	68	68
T3	73	72	65	68	65
T4	68	73	66	70	70

Table 1: Measured dimensions of printed columns.

EXPERIMENTAL SETUP

All six columns were tested in a three-point bending configuration using a steel loading frame at the AdMaS Centre, Brno University of Technology. Compliant rubber layers were placed on the supports to prevent local damage caused by surface irregularities. The columns were loaded at mid-span using a hydraulic press. Deflection at the load point was monitored with a laser displacement sensor, while force and displacement were recorded continuously throughout the loading process. Each test was terminated upon structural failure.

The specimens exhibited different stiffness and peak loads, primarily due to variations in print quality and interlayer bonding. In this study, six 3D-printed concrete columns were intentionally fabricated with imperfections to simulate defects likely to occur in real construction. Prior to loading, each element was digitized using a structured-light 3D scanner. Destructive bending tests were then carried out, and the observed failure modes were analysed with respect to geometry and defect position. Following the tests, fragments were extracted from the failed columns for additional laboratory evaluation of mechanical and physical properties, including compressive strength, flexural tensile strength in both parallel and perpendicular directions, ultrasonic pulse velocity, bulk density, and water absorption.

After failure, fragments were cut from the tested columns to represent different areas and orientations of the original print. They were marked according to their orientation (parallel or perpendicular to print layers) and labelled for subsequent evaluation. The bending test configuration is illustrated in Fig. 2a, b. Examples of the fractured specimen after the bending tests are illustrated in Figs. 3 and 4.

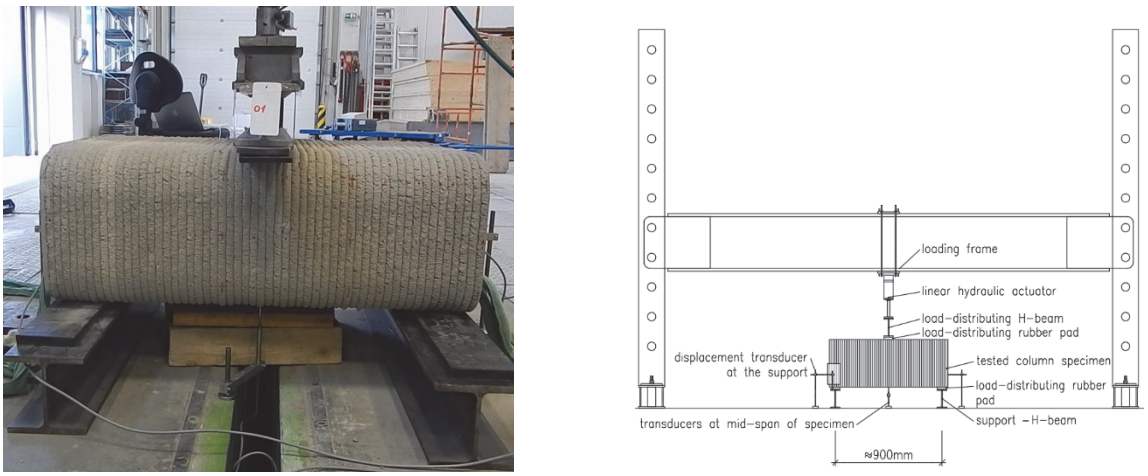

(a) (b)

Figure 2: Experiment setup: a) Photo of specimen placed in the loading setup; b) Scheme of position of sensors and loading press head.

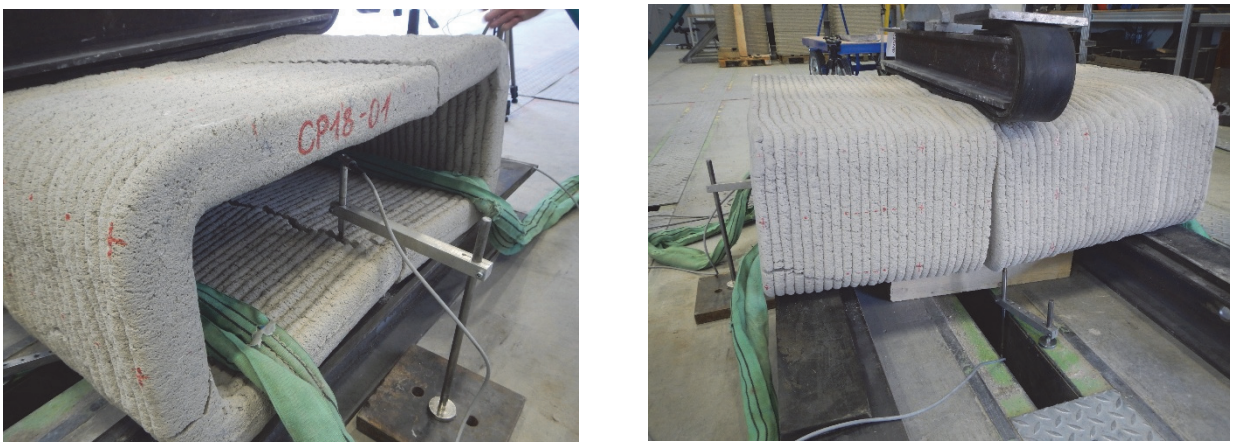

(a) (b)

Figure 3: a) Fractured specimen CP18-01; b) Fractured specimen CP18-02.

Once each bending test reached the failure point, fragments were removed from the broken halves of the columns using a diamond saw. Where possible, fragments were shaped into regular geometries, with minor deviations from ideal shapes accepted in order to retain sufficient specimen size for standardised tests. Examples of fragment specimens are shown in Fig. 5.

Each fragment was tested for several mechanical and physical parameters. Compressive strength was determined according to EN 12390-3 using cube specimens [3]. Flexural tensile strength was measured in three-point bending according to EN 12390-5, with specimens tested both parallel and perpendicular to the print layers [1]. Bulk density was determined by hydrostatic weighing in accordance with ČSN EN 12390-7[1]. Water absorption was evaluated by soaking dried specimens in water and recording weight gain after 48 hours. All tests were performed according to the relevant standards, with minor adaptations for the geometry and surface characteristics of the 3D-printed material.

(a) (b)

Figure 4: a) Fractured specimen CP18-03; b) Fractured specimen CP18-04.

Figure 5: Extracted sub-sections of walls from the 3D printed test specimens.

NUMERICAL MODELLING

A simplified finite element (FEM) model was developed to reproduce the bending response of the full-scale printed columns. The geometry was idealized as a rectangular hollow section derived from the average measured dimensions. Linear elastic material behaviour was assumed, while interlayer interfaces between printed filaments were represented by surface-based cohesive elements. Material parameters were initially obtained from fragment testing and subsequently calibrated to reproduce the load–deflection response observed in the experiments.

Parameter	Value	Note
Elastic modulus E	9 000 – 30 320 Mpa	Wide range due to different failure mechanisms observed experimentally; calibrated in model
Poisson's ratio μ	0.20	Literature value
Bulk density ϱ	2100 – 2250 kg/m³	Measured on fragments
Compressive strength f_c	16.6–32.2 Mpa	Based on fragment tests
Tensile strength f_t	15 Mpa	Intentionally higher than real to prevent premature failure in the model

Table 2: Input parameters of the simplified FEM model.

FULL-SCALE BENDING TEST RESULTS

All six columns were tested in a three-point bending configuration using a steel loading frame at the AdMaS Centre, Brno University of Technology. Compliant rubber layers were placed on the supports to prevent local damage caused by surface irregularities. The columns were loaded at mid-span using a hydraulic press. Deflection at the load point was monitored with a laser displacement sensor, while force and displacement were recorded continuously throughout the loading process. Each test was terminated upon structural failure. The evolution of force-deflection diagram of all specimens is shown in Fig. 6, where on x axis is deflection in mm and on y axis is bending force in kN.

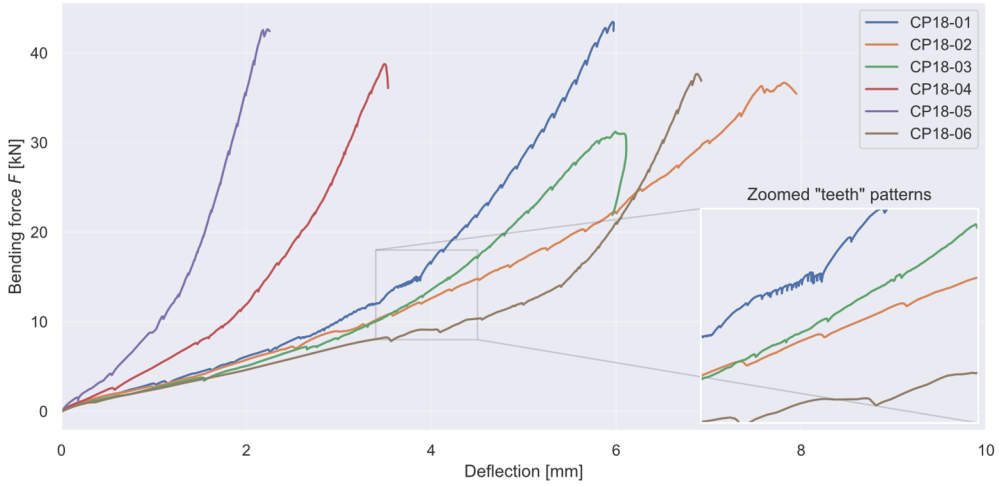

Figure 6: Force deflection diagram of tested specimens with visible "teeth" patterns.

Three of the specimens exhibited gradual bending failure, with a tensile crack developing at the bottom surface. The remaining three failed suddenly and in a brittle manner, initiated by delamination along interlayer interfaces. These results highlight the pronounced anisotropy of the material and its sensitivity to interlayer bonding quality. Significant variability in peak load and stiffness was also observed, governed by local defects, printing irregularities, and print orientation. Columns with more uniform print quality and minimal visible gaps between layers reached higher load capacities and showed more stable failure modes. Conversely, specimens with rough surfaces and visible cold joints exhibited earlier and more abrupt failure. Flexural tensile strength was consistently higher parallel to the print direction, whereas perpendicular specimens tended to fail along layer boundaries due to delamination. The mean values were 1.96 MPa (parallel) and 1.27 MPa (perpendicular).

FRAGMENT TESTING RESULTS

The fragments were produced by cutting prismatic and cubic specimens from the failed full-scale 3D-printed columns using a diamond saw. Their surfaces were ground to obtain regular shapes while maintaining the original printing orientation. Each column provided a set of six beam specimens (three tested parallel and three perpendicular to the

print layers) and six cubes. The beam specimens measured approximately 65 × 65 × 200 mm, and the cubes 65 × 65 × 65 mm. These dimensions were chosen according to the filament width of the printed material, representing one wall thickness of the original columns. The preparation procedure ensured that the orientation and characteristic features of the printed layers were preserved for subsequent mechanical testing. The specimen types and preparation steps are illustrated in Fig. 5. Prior to testing, all specimens were measured with a caliper and digitised using a structured-light 3D scanner to capture their actual geometry and potential surface irregularities. The tests were performed in the Structural Testing Laboratory of the Faculty of Civil Engineering, Brno University of Technology. Compressive strength tests were carried out on cubic specimens in accordance with EN 12390-3, using a hydraulic testing machine at a loading rate of 0.6 ± 0.2 MPa/s, which corresponds to approximately 3 kN/s for a 68 mm cube. Each specimen was oriented either parallel or perpendicular to the printed layers to observe anisotropy effects.

Flexural tensile strength tests were conducted on beam specimens in a three-point bending configuration following EN 12390-5. The span between supports was 250 mm, and the loading rate corresponded to a stress increase of 0.05 MPa/s. The tests were performed using a hydraulic press equipped with three cylindrical supports, and the applied force was recorded continuously until failure. The beams were tested both parallel and perpendicular to the print direction to evaluate interlayer bonding.

Bulk density was determined by hydrostatic weighing in accordance with EN 12390-7, while water absorption was measured by immersing dried specimens in water for 48 hours and recording mass gain. Ultrasonic pulse velocity (UPV) was measured both along and across the print layers using the transmission method to assess internal continuity and potential delamination zones.

All test procedures followed the respective standards but were slightly modified to account for the specific geometry and layered nature of 3D-printed concrete. The adopted methodology ensured that all results could be directly compared between orientations and with reference values for conventionally cast concrete. The test results were stored in Zenodo repository and are available under BSD license [8].

The extracted fragments were subjected to compression, flexural tension, bulk density, water absorption, and ultrasonic pulse velocity testing. All measured properties exhibited a clear directional dependence between specimen loaded parallel and perpendicular to the print layers. An illustration of the prepared specimens is provided in Fig. 7.

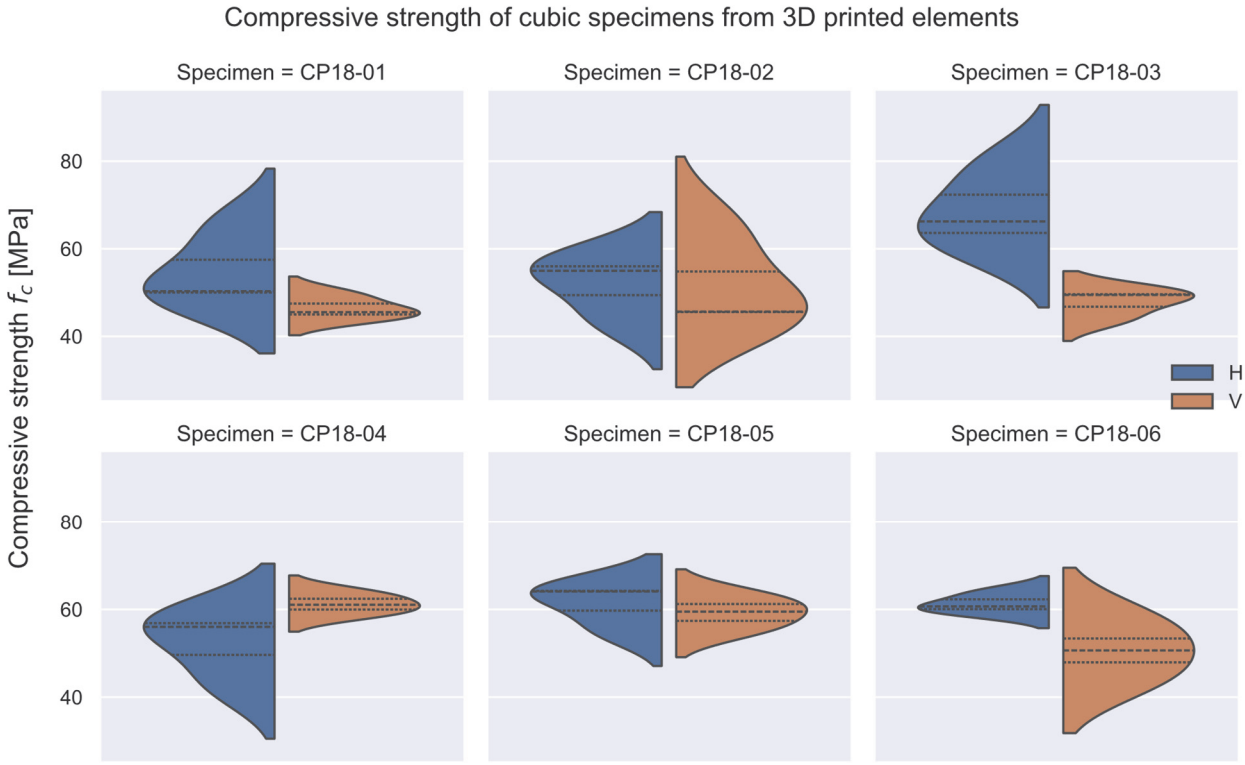

Figure 7: Effect of horizontal (*H)* and vertical (V) loading of cubes cut out of the 3D printed specimen.

FINITE ELEMENT ANALYSIS

Numerical simulations were carried out in Atena/GiD using tetrahedral elements. The models were defined as purely linear elastic, with the primary objective of reproducing the global stiffness and deflection response observed in the experiments. Nonlinear fracture parameters and energy release mechanisms were not considered, since the available experimental dataset consisted only of vertical displacements at the supports and mid-span, recorded by two sensors. This limited amount of data did not justify calibration of detailed stress fields or crack propagation.

The elastic modulus E applied in the simulations spanned a wide range (9–30 GPa). This variation reflected both the simplified modelling assumptions and the experimental variability, where different failure mechanisms occurred among the printed columns. The tensile modulus had the strongest influence on deflection behaviour; however, within the isotropic model it was not possible to distinguish tensile from compressive stiffness. For comparison, modulus values estimated from ultrasonic pulse velocity on fragments differed considerably from those back-calculated in the FEM calibration. This discrepancy highlights both the limitations of ultrasonic evaluation in anisotropic materials and the simplifications inherent in the adopted model.

Supports were represented as elastic blocks with constant stiffness ($\mu = 0.30$), ensuring that their deformation had no significant influence on the structural response. The tensile strength was intentionally set higher than experimentally measured values to avoid premature numerical failure, since the main objective was to reproduce the overall load–deflection trend rather than the precise failure mode.

The simplified FEM approach successfully reproduced the initial stiffness and the general load–deflection shape but could not capture brittle delamination or anisotropic crack propagation observed in experiments. This was an expected outcome of the modelling simplifications. Nevertheless, the results confirm that even a basic linear-elastic model, when supported by experimental calibration, can provide valuable insight into the global mechanical behaviour of 3D-printed concrete elements.

The main purpose of the finite element (FEM) study was to verify whether a simplified linear-elastic numerical model could reproduce the global stiffness and deflection behaviour observed during the full-scale bending tests. Rather than predicting the exact failure mechanism, the model served as a tool for evaluating how the layered geometry and the assumed interfacial stiffness influence the overall structural response of the printed elements.

To assess agreement with the experimental data, the load–deflection curves obtained from the FEM analysis were compared with those recorded during the bending tests (Fig. 8a). The maximum load levels predicted by the model (5.8 – 7.2 kN) were within approximately 10–15 % of the experimental peak loads (6.2 – 7.5 kN), and the initial stiffness matched the measured slope of the curve closely. However, the model was unable to capture the sudden post-peak drop in load associated with interlayer delamination and brittle fracture, phenomena that cannot be represented in a purely linear-elastic analysis.

Despite these simplifications, the FEM results provided valuable insight into the influence of interlayer bonding stiffness and confirmed that the global structural response of 3D-printed concrete elements can be reasonably reproduced when appropriate material calibration is applied. The study therefore demonstrates the potential of simplified numerical models as an efficient diagnostic and predictive tool for assessing the mechanical behaviour of additively manufactured concrete structures.

The FEM plots help rationalise the two dominant experimental failure modes. In geometrically regular columns (e.g., CP18-01, CP18-03, CP18-06), the σ_{yy} field (Fig. 8d) concentrates at mid-span in the tension zone, which matches the flexural crack initiating at the bottom surface and a gradual loss of stiffness recorded during the tests. Conversely, in columns with print-related imperfections (notably CP18-04 with a locally narrower filament along one-third of the span and CP18-05 with a reduced filament width on one long side, located on the upper side during loading), the σ_{xx} field (Fig. 8b) shows elevated stresses across the wall thickness directly beneath the loading head and along the upper wall. These stress concentrations, amplified by geometric discontinuities and interlayer weakness, are consistent with the punch-through/local crushing of the top wall and delamination-triggered brittle failure observed in the laboratory. The σ_{zz} map (Fig. 8c) further clarifies the diagonal compression-strut path between the load and supports; any local loss of stiffness along this path (e.g., reduced filament width or imperfect interlayer bonding) shifts stresses towards the upper shell, increasing the likelihood of non-flexural failure.

Taken together, the FEM visualisations (a–d) (i) explain why ideal geometry favours classic flexural failure at mid-span, while (ii) local geometric defects introduce parasitic through-thickness stresses that precipitate top-wall breach or interlayer delamination. This interpretation is consistent with the specimen-specific observations: CP18-01/03/06 → flexural crack at mid-span; CP18-04/05 → premature top-wall failure aligned with the defective strip; CP18-02 → lower flexural capacity and mixed behaviour, reflecting its greater geometric variability.

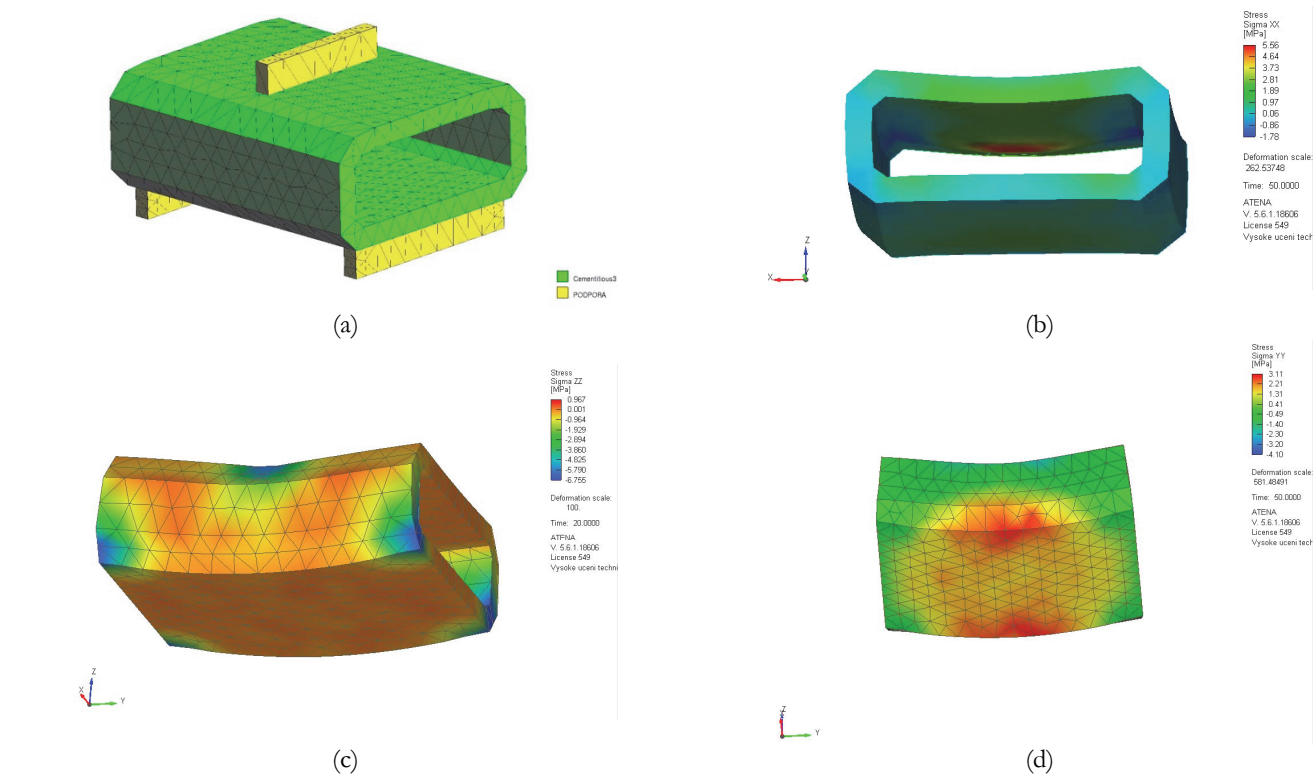

Figure 8: Finite-element visualization of the three-point bending test. (a) Idealised model in Atena with the finite-element mesh.; (b) Normal stress σ_{xx} (horizontal, across the wall thickness). Note the local increase under the loading head and along the upper wall at mid-span; in specimens with imperfect geometry this correlates with the punch-through of the top wall observed experimentally.; (c) Normal stress σ_{zz} (vertical). The stress field follows a compression strut between the loading point and the supports, illustrating how the load is transferred diagonally through the shell; (d) Normal stress σ_{yy} (longitudinal, along the span). Peak tensile stresses occur at mid-span at the bottom fibre, in agreement with flexural cracking observed on geometrically regular specimens.

COMPARISON OF RESULTS

Due to the limited number of specimens, a full statistical evaluation was not feasible. Nevertheless, several clear relationships between the measured properties were identified:

- Water absorption vs. compressive strength – An inverse trend was observed: more porous specimens with higher absorption exhibited lower compressive strength, most likely due to reduced compactness and weaker interlayer bonding.
- Bulk density vs. strength – Higher density generally corresponded to improved mechanical performance. The strongest correlation was identified for flexural strength in the direction parallel to the print path.
- Ultrasonic pulse velocity vs. strength – A good correlation was found with both compressive strength and elastic modulus, indicating that ultrasonic methods can serve as a useful indirect tool for detecting internal defects.
- Print direction vs. flexural strength – Specimens tested along the print layers demonstrated higher and more stable strength, whereas those tested across the layers showed lower values and more variability. This confirms the pronounced anisotropy of the printed material and underlines the necessity of standardised testing directions.

By combining these parameters, a more robust diagnostic methodology can be developed. For instance, integrating ultrasonic pulse velocity with bulk density data may enable the approximate identification of weaker zones in real structures, thus opening the way toward predictive in-situ assessment and quality control.

Quantitative evaluation of the experimental results supports the qualitative trends discussed above. The flexural tensile strength measured parallel to the print layers averaged 1.96 MPa, while specimens tested perpendicular to the layers averaged 1.27 MPa, representing an increase of approximately 35 % in the parallel direction. The lowest recorded perpendicular value of 0.56 MPa corresponds to a reduction of nearly 70 % compared with the best-performing parallel specimens. In compression, the effect of orientation was less pronounced: mean values ranged from 16.6 MPa to 32.2 MPa, with a

coefficient of variation of about 25 %, suggesting that compressive performance is governed primarily by local density rather than by layer orientation.

Ultrasonic pulse velocity showed an average reduction of approximately 400 m/s (around 7 %) across the print layers compared with the parallel direction, confirming weaker interlayer bonding. Likewise, water absorption increased from 5–7 % for dense, well-bonded specimens to 7–9 % for those exhibiting visible layer separation, corresponding to a 25–30 % rise in apparent porosity. These quantitative comparisons substantiate the observed anisotropy and demonstrate that orientation-related differences in both strength and physical parameters are statistically meaningful, even within the limited set of tested specimens.

Following the destructive bending tests of the full-scale columns, fragments were extracted for detailed laboratory investigation. Standardized procedures were applied with minor adaptations to account for geometry and surface characteristics: compressive strength, flexural tensile strength in both principal directions, bulk density, water absorption, and ultrasonic pulse velocity. Special attention was given to the orientation of flexural tests, as loading direction relative to the print layers had a decisive influence on performance.

Fragments tested parallel to the print path consistently achieved higher and more uniform tensile strengths compared to those tested across the layers, where delamination and interlayer separation occurred more frequently. Ultrasonic measurements (direct transmission) likewise revealed orientation-dependent variations in wave speed, reflecting the condition of the internal interfaces. These results were subsequently employed in the correlation analysis.

The illustration of cross corelation of selected parameters is shown in Fig. 9 where selected parameters Absorbance A, density D, bending force Fct and compressive strength fc is shown in cross corelation pattern. At diagonal axis the histogram with KDE (kernel density estimate) analysis is shown. In the upper side of mirrored cross plot, a corelation in terms of Pearson coefficient is calculated for paired variables by row and column of the diagram.

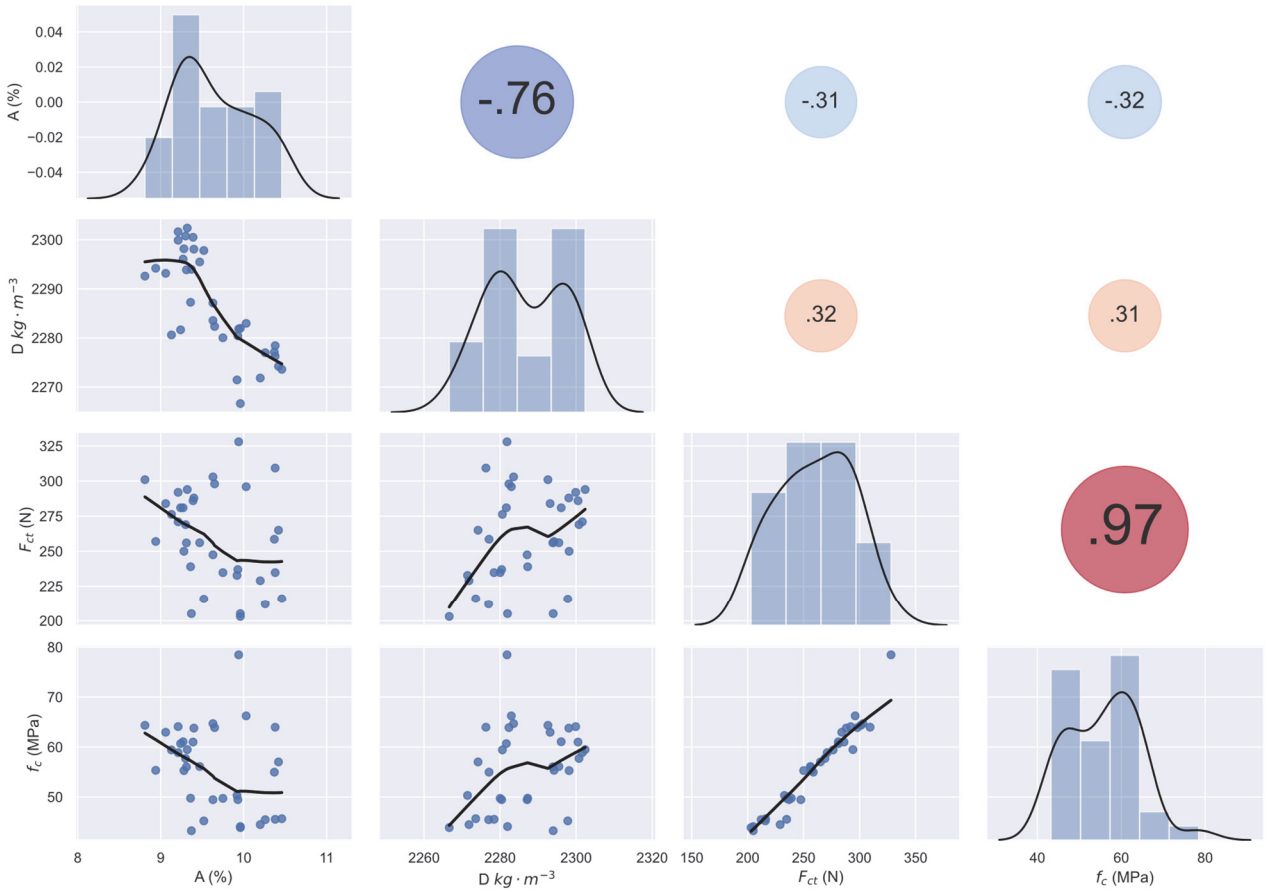

Figure 9: Cross dependency of measured properties.

The highest correlation for specimens is observed between compressive strength and bending force during 3-point bending tests. The density and strength and force parameters are at value 0.31 and 0.32 which indicates that those three parameters are not in correlation, which is expected and nicely illustrates the shape characteristics of columns. The indirect dependency

between absorbality and density is at -0.76 which indicates that lowering absorbance relates to more dense structure of 3D printed elements.

DISCUSSION

The experimental results confirmed that 3D-printed concrete (3DCP) exhibits markedly different behaviour compared to conventionally cast concrete. The most significant finding was the pronounced mechanical anisotropy, particularly evident in tensile strength and ultrasonic wave propagation. Specimens loaded parallel to the print direction achieved higher strength and showed less variability, indicating that interlayer bonding plays a decisive role in overall performance.

The difference in flexural tensile strength between orientations was substantial:

- Average parallel: 1.96 MPa
- Average perpendicular: 1.27 MPa

This corresponds to a reduction of more than 35 % when loaded across the print layers. The lowest recorded perpendicular value (0.56 MPa) highlights the presence of weak planes caused by insufficient adhesion between layers. Ultrasonic pulse velocity measurements supported this conclusion, as wave speed was on average 400 m/s lower in the perpendicular direction. This method therefore appears suitable for detecting internal defects and identifying weak interlayer bonding in printed structures.

In compression, the material demonstrated comparatively stable behaviour, with a mean strength of 25.3 MPa. Nevertheless, several fragments dropped below 20 MPa, raising concerns for structural applications. These weaker results were typically associated with lower bulk density and higher water absorption. Clear correlations were observed between physical and mechanical properties:

- Higher bulk density (up to 2.211 kg/m³) generally correlated with higher compressive strength.
- Increased water absorption (above 7 %) was usually linked to lower strength values.

Such trends support the use of physical tests—density, absorption, and ultrasonic velocity—for indirect evaluation of mechanical performance, particularly when destructive testing is not feasible.

The variability among specimens also explained the differing failure modes in the full-scale bending tests. Columns with higher print quality showed gradual crack development and higher peak load, while those with weaker interlayer bonding failed suddenly and at lower loads. This demonstrates that visual inspection or surface-based diagnostics alone may be insufficient.

Overall, the findings emphasize that reliable diagnostics of 3DCP structures must account for print orientation, internal defects, and material variability. Existing concrete standards are not directly applicable and need to be adapted to the specific characteristics of additive manufacturing.

CONCLUSION

The experiments confirmed that 3D-printed concrete elements behave differently from conventionally cast specimens. The layered nature of the material introduces anisotropy, which strongly influences flexural and tensile performance. Failure modes were governed not only by material quality but also by geometric accuracy and print-induced defects. Testing of extracted fragments provided a more detailed quantification of mechanical and physical properties, while correlation analysis revealed strong links between density, absorption, ultrasonic velocity, and strength parameters. These findings support the integration of indirect testing methods into a comprehensive diagnostic toolkit.

For structural testing and assessment, 3DCP poses unique challenges that cannot be addressed by conventional procedures. A combined approach using scanning, experimental testing, and numerical simulation appears promising for reliable verification. The data presented in this study may serve as a foundation for future diagnostic guidelines applicable to both laboratory and field conditions.

The following main conclusions can be drawn:

- Anisotropy as a key feature – Tensile strength and ultrasonic velocity were significantly lower perpendicular to the print layers, confirming that interlayer bonding is the weak point of the material.
- Flexural tensile strength – A reduction of more than 35 % was observed across layers compared to the parallel direction.
- Premature failure – Several specimens failed at very low stresses due to interlayer delamination.

- Compressive strength – More stable, but still variable, in the range of 16.6–32.2 MPa. The average of 25.3 MPa demonstrates that structural-grade strength is achievable under good printing conditions.
- Physical properties as indicators – Bulk density and water absorption showed clear correlations with mechanical performance and may serve as diagnostic indicators for quality assessment.
- Ultrasonic evaluation – Ultrasonic pulse velocity proved effective for detecting weak interlayer zones and has strong potential for non-destructive evaluation.
- Numerical modelling – A simplified FEM approach, calibrated with fragment testing, reproduced the global load–deflection behaviour and confirmed the role of cohesive layer properties in structural response.

The proposed experimental and diagnostic methodology provides a framework for future quality control and structural evaluation of 3D-printed concrete elements. Further research should aim at developing adapted testing standards and addressing long-term durability and reliability aspects of 3DCP structures.

ACKNOWLEDGEMENTS

This publication was financed by the internal standard project of Brno University of Technology, Faculty of Civil Engineering under No. FAST-S-25-8820.

REFERENCES

[1] ČSN EN 12390-7 (731302) Zkoušení ztvrdlého betonu - Část 7: Objemová hmotnost ztvrdlého betonu. (2009).
[2] Alami, A.H., Olabi, A.G., Ayoub, M., Aljaghoub, H., Alasad, S., Abdelkareem, M.A. (2023). 3D Concrete Printing: Recent Progress, Applications, Challenges, and Role in Achieving Sustainable Development Goals, Buildings, 13(4), p. 924. DOI: https://doi.org/10.3390/buildings13040924.
[3] ČSN EN 12390-3 (731302) Zkoušení Ztvrdlého Betonu - Část 3: Pevnost v Tlaku Zkušebních Těles. (2009).
[4] Le, T.T., Austin, S.A., Lim, S., Buswell, R.A., Law, R., Gibb, A.G.F., Thorpe, T. (2012). Hardened properties of high-performance printing concrete, Cem Concr Res, 42(3), pp. 558–566. DOI: https://doi.org/10.1016/j.cemconres.2011.12.003.
[5] Ma, G., Li, Z., Wang, L., Wang, F., Sanjayan, J. (2019). Mechanical anisotropy of aligned fiber reinforced composite for extrusion-based 3D printing, Constr Build Mater, 202, pp. 770–783. DOI: https://doi.org/10.1016/j.conbuildmat.2019.01.038.
[6] Miller, S.A., Horvath, A., Monteiro, P.J.M. (2018). Impacts of booming concrete production on water resources worldwide, Nat Sustain, 1(1), pp. 69–76. DOI: https://doi.org/10.1038/s41893-017-0009-5.
[7] Skibicki, S., Dvořák, R., Pazdera, L., Topolář, L., Kocáb, D., Alexa, M., Cendrowski, K., Hoffmann, M. (2024). Anisotropic mechanical properties of 3D printed mortar determined by standard flexural and compression test and acoustic emission, Constr Build Mater, 352, p. 138957. DOI: https://doi.org/10.1016/j.conbuildmat.2024.138957.
[8] Zareiyan, B., Khoshnevis, B. (2017). Effects of interlocking on interlayer adhesion and strength of structures in 3D print.